

Exclusive $\Xi\Xi$ and $\Xi_c\Xi_c$ production in $\bar{p}p$ collisions at $\sqrt{s} \lesssim 15$ GeV

A.I. Titov^{a,b} and B. Kampfer^{a,c}

^a Helmholtz-Zentrum Dresden-Rossendorf, 01314 Dresden, Germany

^b Bogoliubov Laboratory of Theoretical Physics, JINR, Dubna 141980, Russia

^c Institut für Theoretische Physik, TU Dresden, 01062 Dresden, Germany

Estimates of differential cross sections and longitudinal asymmetries are presented for the reactions $\bar{p}p \rightarrow \Xi\Xi$ and $\bar{p}p \rightarrow \Xi_c\Xi_c$ at energies $\sqrt{s} \lesssim 15$ GeV. The Ξ and Ξ_c hyperons are assumed to be produced in two-step processes: first, intermediate $\bar{\Lambda}\Lambda$ and/or $\bar{\Lambda}_c\Lambda_c$ states are created which are converted afterwards into final states $\Xi\Xi$, $\Xi_c\Xi_c$ and $\Xi_c\Xi_c$. The full amplitudes are described by loop diagrams within a modified Regge model, based on the topological decomposition of planar quark diagrams. A strong sensitivity of the ratio of yields of $\Xi_c\Xi_c$ to $\Xi\Xi$ and of $\bar{\Lambda}_c\Lambda_c$ to $\bar{\Lambda}\Lambda$ to the degree of SU(4) symmetry violation is found.

PACS numbers: 13.85.-t, 11.80.-m, 11.55.Jy

Open charm production will be one of the major topics of the hadron and heavy-ion programmes at the planned Facility for Anti-proton and Ion Research (FAIR) [1]. Charm spectroscopy will be addressed by the PANDA Collaboration [2] in reactions induced by anti-protons, while the CBM Collaboration [3] will exploit charmed hadrons as probes of the nuclear medium at maximum compression in heavy-ion collisions. For both large-scale experiments at FAIR one needs to know the properties of charmed baryons as well as their production processes in elementary pp and $\bar{p}p$ reactions. The opportunities at FAIR are promising. For instance, the PAX Collaboration [4] envisages the use of a polarized anti-proton beam. This offers the chance to study in depth the mechanism of open charm production at energies from the thresholds to $\sqrt{s} \lesssim 15$ GeV.

In [5] we have estimated the open charm production in the exclusive binary reactions $\bar{p}p \rightarrow \bar{Y}Y_c$ ($Y = \Lambda, \Sigma$), $\bar{p}p \rightarrow D\bar{D}$ and $\bar{p}p \rightarrow D\bar{D}^*$ at small momentum transfer. We developed a modified Regge type model, motivated by quark-gluon string dynamics [6]. Important ingredients of the model [5] are the effective charmed meson and baryon exchange trajectories as well as the energy scale parameters. They are found from a consistent approach based on the topological decomposition and factorization of the corresponding planar quark diagrams. The coupling constants are taken to be the same as in corresponding strangeness production reactions, i.e. assuming SU(4) symmetry. Unknown residual functions are found from a comparison of $\bar{p}p \rightarrow \bar{\Lambda}\Lambda$ and $\bar{p}p \rightarrow \bar{\Lambda}\Sigma$ reactions with available experimental data. As a result, the corresponding cross sections in the energy range of future FAIR experiments are obtained. For other approaches to the $\bar{\Lambda}_c\Lambda_c$ production in $\bar{p}p$ collisions we refer the interested reader to [7, 8].

The aim of our present study is to extend the model [5] for studying the production of the doubly-strange baryon Ξ ($\Xi^0 = (uss)$, $\Xi^- = (dss)$) and the strange-charm baryon Ξ_c ($\Xi_c^+ = (usc)$, $\Xi_c^0 = (dsc)$) in peripheral $\bar{p}p$ collisions. We assume that the Ξ (Ξ_c) hyperons are produced in two-step processes, where the first step corre-

sponds to the creation of intermediate $\bar{\Lambda}\Lambda$ ($\bar{\Lambda}_c\Lambda_c$) states. The Ξ (Ξ_c) hyperons are produced then in a second step due to the final state interactions $\bar{\Lambda}\Lambda \rightarrow \Xi\Xi$, $\bar{\Lambda}\Lambda \rightarrow \Xi_c\Xi_c$ and $\bar{\Lambda}_c\Lambda_c \rightarrow \Xi_c\Xi_c$ for which we employ the same formalism which was used previously in [5] for description of $\bar{p}p \rightarrow \bar{\Lambda}\Lambda$ and $\bar{p}p \rightarrow \bar{\Lambda}_c\Lambda_c$ reactions. To fix parameters we assume, for a benchmark calculation, the validity of SU(4) symmetry. However, since the probability of the reaction $\bar{p}p \rightarrow \Xi_c\Xi_c$ is sensitive to the degree of SU(4) violation we analyze the dependence of the ratios of $\Xi_c\Xi_c$ to $\Xi\Xi$ and of $\bar{\Lambda}_c\Lambda_c$ to $\bar{\Lambda}\Lambda$ yields on a parameter which describes the degree of SU(4) symmetry violation. Furthermore, we evaluate the longitudinal asymmetry for $\bar{p}p \rightarrow \Xi\Xi$ and $\bar{p}p \rightarrow \Xi_c\Xi_c$ reactions.

The amplitudes of the $\Xi\Xi$ and $\Xi_c\Xi_c$ production are described by the loop diagrams depicted in Fig. 1 (a) and (b), respectively. Intermediate Λ 's or/and Λ_c 's are pro-

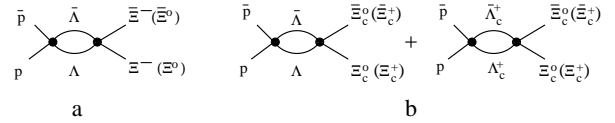


FIG. 1: Loop diagrams for $\Xi\Xi$ (a) and $\Xi_c\Xi_c$ (b) production in peripheral $\bar{p}p$ collisions.

duced in a first step. In principle, one has to include also diagrams with intermediate $\bar{\Lambda}\Sigma$ and $\bar{\Sigma}\Sigma$ configurations. However, their contributions are strongly suppressed due to SU(3) symmetry arguments [5], and, therefore, we skip them. The Ξ and Ξ_c hyperons are produced in a second step due to the final state interactions $\bar{\Lambda}\Lambda \rightarrow \Xi\Xi$ and $\bar{\Lambda}_c\Lambda_c \rightarrow \Xi_c\Xi_c$. Since in the considered peripheral reactions the momentum transfer is relatively small, the intermediate $\bar{\Lambda}\Lambda$ ($\bar{\Lambda}_c\Lambda_c$) hyperons are almost on-shell. This fact allows one to approximate the total amplitudes of $\bar{p}p \rightarrow \bar{\Lambda}\Lambda \rightarrow \Xi\Xi$ and $\bar{p}p \rightarrow \bar{\Lambda}\Lambda, \bar{\Lambda}_c\Lambda_c \rightarrow \Xi_c\Xi_c$ reactions by contributions of the corresponding pole parts depicted in Fig. 2. The pole parts of the box diagram (right panel in Fig. 2) are calculated in a straightforward manner by using Cutkosky cutting rules [9]. Thus, for

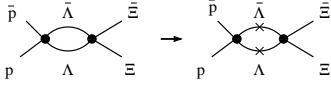


FIG. 2: Cut (pole) diagram for the reaction $\bar{p}p \rightarrow \bar{\Lambda}\Lambda \rightarrow \bar{\Xi}\Xi$.

reaction $\bar{p}p \rightarrow \bar{\Xi}\Xi$ one has

$$\begin{aligned} T^{\bar{p}p \rightarrow \bar{\Xi}\Xi} &\simeq T^{\bar{p}p \rightarrow \bar{\Xi}\Xi}_{\text{cut}} \\ &= i \frac{Q_\Lambda}{8\pi\sqrt{s}} \int \frac{d\Omega_\Lambda}{4\pi} \sum_{\text{spins } \bar{\Lambda}\Lambda} T^{\bar{p}p \rightarrow \bar{\Lambda}\Lambda} T^{\bar{\Lambda}\Lambda \rightarrow \bar{\Xi}\Xi}, \quad (1) \end{aligned}$$

where Q_Λ and Ω_Λ are the three momentum and solid angle of the intermediate Λ hyperon in the center-of-mass system (c.m.s.), respectively; the Mandelstam variable s denotes the square of the total energy. $T^{\bar{p}p \rightarrow \bar{\Lambda}\Lambda}$ and $T^{\bar{\Lambda}\Lambda \rightarrow \bar{\Xi}\Xi}$ are the amplitudes of the $\bar{p}p \rightarrow \bar{\Lambda}\Lambda$ and $\bar{\Lambda}\Lambda \rightarrow \bar{\Xi}\Xi$ processes, respectively. The amplitude for $\bar{p}p \rightarrow \bar{\Xi}_c\Xi_c$ reaction is similar, but here we have a coherent superposition of intermediate $\bar{\Lambda}\Lambda$ and $\bar{\Lambda}_c\Lambda_c$ in accordance with Fig. 1 (b).

The partial amplitudes $T^{\bar{Y}Y \rightarrow \bar{Y}'Y'}$ where the flavor content of spin- $\frac{1}{2}$ baryons Y, Y' changes by one unit has been considered in [5] in a model based on the quark-gluon string dynamics [6]. These amplitudes are described by planar quark diagrams. Examples for $\bar{\Lambda}\Lambda \rightarrow \bar{\Xi}\Xi$ and $\bar{\Lambda}_c\Lambda_c \rightarrow \bar{\Xi}_c\Xi_c$ are depicted in Fig. 3 (a) and (b), respectively. These amplitudes have the form of a

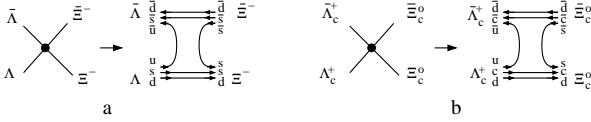


FIG. 3: Planar quark diagrams for $\bar{\Lambda}\Lambda \rightarrow \bar{\Xi}\Xi$ (a) and $\bar{\Lambda}_c\Lambda_c \rightarrow \bar{\Xi}_c\Xi_c$ (b) transitions.

Regge pole amplitude dominated by the vector meson ($V = K^*, D^*$) exchange

$$\begin{aligned} T^{\bar{Y}Y \rightarrow \bar{Y}'Y'}_{m_f n_f; m_i n_i} &= C(t) \mathcal{M}^{\bar{Y}Y \rightarrow \bar{Y}'Y'}_{m_f n_f; m_i n_i}(s, t) \frac{g_{VYY'}}{s_0} \\ &\times \Gamma(1 - \alpha_V(t)) \left(-\frac{s}{s_{\bar{Y}Y; \bar{Y}'Y'}} \right)^{\alpha_V(t)-1}, \quad (2) \end{aligned}$$

where m_i, m_f, n_i and n_f are the spin projections of Y, Y', \bar{Y} , and \bar{Y}' , respectively, $\alpha_V(t)$ is the effective V meson trajectory, $g_{VYY'}$ stands for the coupling constant of the VYY' interaction, and $s_0 = 1$ GeV is a universal scale parameter. The overall residual function $C(t)$ depends solely on the Madelstam variable t and is determined [5] by a comparison with available experimental data of the $\bar{p}p \rightarrow \bar{\Lambda}\Lambda$ reaction as $C(t) = 0.37/(1 - t/1.15)^2$. The flavor content of the exchanged vector meson V is $(\bar{q}f)$ with $q = u, d$ and $f = s, c$.

In our consideration we use the nonlinear representation for the meson trajectories developed in [10],

$$\alpha(t) = \alpha(0) + \gamma(\sqrt{T} - \sqrt{T-t}), \quad (3)$$

where $\gamma = 3.65$ GeV $^{-1}$ is the universal parameter (i.e. the slope of the asymptotic region), and $T \gg 1$ GeV 2 is the scale parameter, being special for each trajectory. In the diffractive region with $-t \ll T$, the linear approximation $\alpha(t) = \alpha(0) + \alpha't$ with $\alpha' \simeq \gamma/2\sqrt{T}$ is valid. In our numerical calculations we employ $\alpha_V(t)$ with $V = K^*, D^*$ and $\rho, \phi, J/\psi$ from [5], where the later three trajectories are used for the evaluation of the energy scale parameters $s_{\bar{Y}Y; \bar{Y}'Y'}$ in Eq. (2). These parameters are related to the corresponding scale parameters for the diagonal transitions $\bar{Y}Y \rightarrow \bar{Y}Y$ (for $s_{\bar{Y}Y; \bar{Y}Y}$) and $\bar{Y}'Y' \rightarrow \bar{Y}'Y'$ (for $s_{\bar{Y}'Y'; \bar{Y}'Y'}$). Thus, for example, for $\bar{\Lambda}\Lambda \rightarrow \bar{\Xi}_c\Xi_c$ and $\bar{\Lambda}_c\Lambda_c \rightarrow \bar{\Xi}_c\Xi_c$ transitions:

$$\begin{aligned} s_{\bar{\Lambda}\Lambda; \bar{\Xi}_c\Xi_c}^{2(\alpha_{D^*}(0)-1)} &= s_{\bar{\Lambda}\Lambda}^{\alpha_{\rho}(0)-1} s_{\bar{\Xi}_c\Xi_c}^{\alpha_{J/\psi}(0)-1}, \\ s_{\bar{\Lambda}_c\Lambda_c; \bar{\Xi}_c\Xi_c}^{2(\alpha_{K^*}(0)-1)} &= s_{\bar{\Lambda}_c\Lambda_c}^{\alpha_{\rho}(0)-1} s_{\bar{\Xi}_c\Xi_c}^{\alpha_{\phi}(0)-1}. \end{aligned}$$

(Here and further on, we use the notation $\Lambda_c \equiv \Lambda_c^+$.) The scale parameters for the diagonal transitions s_{ab} are determined by the sum of the transverse masses of the constituent quarks [6] as $s_{ab} = (\sum_i^{n_a} M_{i\perp})(\sum_j^{n_b} M_{j\perp})$ with $M_{q\perp} \simeq 0.5$ GeV, $M_{s\perp} \simeq 0.6$ GeV, and $M_{c\perp} \simeq 1.6$ GeV. This leads to the following values for the energy scale parameters: $s_{\bar{p}p; \bar{\Lambda}\Lambda} \simeq 2.43$ GeV 2 , $s_{\bar{p}p; \bar{\Lambda}_c\Lambda_c} \simeq 6.0$ GeV 2 , $s_{\bar{\Lambda}\Lambda; \bar{\Xi}\Xi} \simeq 2.75$ GeV 2 , $s_{\bar{\Lambda}\Lambda; \bar{\Xi}_c\Xi_c} \simeq 6.52$ GeV 2 , and $s_{\bar{\Lambda}_c\Lambda_c; \bar{\Xi}_c\Xi_c} \simeq 7.06$ GeV 2 .

The spin dependence in Eq. (2) is accumulated in the amplitude \mathcal{M} which is determined by the symmetry of the VYY' interaction given by the effective Lagrangian

$$\mathcal{L}_{VYY'} = -\bar{Y} \left(\gamma \cdot V - \frac{\kappa VYY'}{M_Y + M_{Y'}} \sigma_{\mu\nu} \partial^\nu V^\mu \right) Y' + \text{h.c.},$$

where Y and Y' denote the baryons (nucleons and hyperons) and $V = K^*, D^*$ the vector meson fields, respectively; κ is the tensor coupling strength. Using this form, one obtains the amplitude \mathcal{M} in Eq. (2)

$$\begin{aligned} \mathcal{M}^{\bar{Y}Y \rightarrow \bar{Y}'Y'}_{m_f n_f; m_i n_i}(s, t) &= \mathcal{N}(s, t) \\ &\times \Gamma_{m_f m_i}^{(Y)\mu} \Gamma_{n_f n_i}^{(\bar{Y})\nu} (-g_{\mu\nu} + \frac{q_\mu q_\nu}{q^2}), \quad (4) \end{aligned}$$

where q is the momentum transfer in the VYY' vertex, $q = p_Y - p_{Y'}$, with p_Y and $p_{Y'}$ as four-momenta of the incoming Y and outgoing Y' baryons, respectively. The functions $\Gamma^{(Y(\bar{Y}))}$ read

$$\Gamma_\mu^{(Y(\bar{Y}))} = \bar{u}_{Y'}(\bar{v}_{\bar{Y}}) \left((1 + \kappa)\gamma_\mu \mp \kappa \frac{(p_Y + p_{Y'})_\mu}{M_Y + M_{Y'}} \right) u_Y(v_{\bar{Y}'})$$

with $\kappa = \kappa_{VYY'}$ and u and v as usual bispinors. The normalization factor $\mathcal{N}(s, t)$ eliminates additional s and t dependencies provided by the Dirac structure in Eq. (4) which is beyond the Regge parametrization:

$$\mathcal{N}(s, t) = \frac{F_\infty(s)}{F(s, t)}, \quad F_\infty(s) = 2s,$$

$$F^2(s, t) = \text{Tr} \left(\Gamma^{(p)} \mu \Gamma^{(p)} \mu'^{\dagger} \right) \text{Tr} \left(\Gamma^{(\bar{p})} \nu \Gamma^{(\bar{p})} \nu'^{\dagger} \right) \\ \times \left(g_{\mu\nu} - \frac{q_{\mu} q_{\nu}}{q^2} \right) \left(g_{\mu'\nu'} - \frac{q_{\mu'} q_{\nu'}}{q^2} \right).$$

For the K^*YY' coupling constants, where Y and Y' belong to the SU(3) baryon octet we use the average values of the Nijmegen potential [11]: $g_{K^*N\Lambda} = -5.18$, $\kappa_{K^*NY} = 2.79$, $g_{K^*\Lambda\Sigma} = -g_{K^*N\Lambda}$ and $\kappa_{K^*\Lambda\Sigma} = 1.03$. For charmed hadrons we employ the following parametrization: $g_{K^*Y_c Y'_c} = g_{D^*YY'_c} = X_{\text{SU}(4)} g_{K^*YY'}$, where the factor $X_{\text{SU}(4)}$ is a measure of the violation of the SU(4) symmetry for charmed hadrons; $X_{\text{SU}(4)} = 1$ means SU(4) symmetry.

The differential cross section $d\sigma/dt$ is related to the invariant amplitude T_{fi} by

$$\frac{d\sigma}{dt} = \frac{1}{16\pi(s - 4M_p^2)^2} |T_{fi}|^2, \quad (5)$$

where summing and averaging over the spin projection in initial and the final state is provided. We also evaluate the longitudinal double-spin asymmetry, defined as

$$\mathcal{A} = \frac{d\sigma^{\Leftarrow} - d\sigma^{\Rightarrow}}{d\sigma^{\Leftarrow} + d\sigma^{\Rightarrow}}, \quad (6)$$

where the symbols \Leftarrow and \Rightarrow correspond to the anti-parallel and parallel spin projections of incoming p and \bar{p} with respect to the quantization axis chosen along the proton momentum in the c.m.s.

Our predictions for differential cross sections of $\bar{p}p \rightarrow \Xi\Xi$ and $\bar{p}p \rightarrow \Xi_c\Xi_c$ reactions are exhibited in Fig. 4 in the left and right panels, respectively. For completeness we also show corresponding results for the cross sections of $\bar{\Lambda}\Lambda$ and $\bar{\Lambda}_c\Lambda_c$ production calculated using Eqs. (2) and (5). The exhibited results are for SU(4) symmetry, i.e. $X_{\text{SU}(4)} = 1$. The cross sections are shown as a function of $t_{\text{max}} - t$, where the square of momentum transfer is $t = (p_p - p_Y)^2$ with $Y = \Xi, \Xi_c, \Lambda, \Lambda_c$, and t_{max} is the maximum value of t which corresponds to the hyperon production at zero angle relative to the momentum of the incoming proton in the c.m.s. In Fig. 4 (left panel) we show the sum of $\Xi^-\Xi^-$ and $\Xi^0\Xi^0$. Since the cross sections for the reactions $\bar{p}p \rightarrow \Xi^-\Xi^-$ and $\bar{p}p \rightarrow \Xi^0\Xi^0$ are almost equal to each other, the corresponding partial contributions are approximately one half of the total cross section. The same is valid for $\Xi_c^0\Xi_c^0$ and $\Xi_c^+\Xi_c^+$. In Fig. 4 (right panel) we show the sum of their partial contributions, being almost equal to each other. One can see the exponential decrease of the cross sections. Their slope is defined by the Regge propagator $(s/s_i)^{2\alpha_V(t)}$, the residual function $C(t)$ and the non-trivial angle dependence of integrand in Eq. (1) for $\Xi\Xi$ ($\Xi_c\Xi_c$) which has a local maximum at $\Omega_{\Lambda} \simeq \Omega_{\Xi}$.

In Fig. 4 (right panel) we show the separate individual contributions of the loop diagrams with intermediate $\bar{\Lambda}\Lambda$ and $\bar{\Lambda}_c^+\Lambda_c^+$ configurations (see Fig. 1 b). The contribution of the diagram with intermediate $\bar{\Lambda}\Lambda$ is suppressed

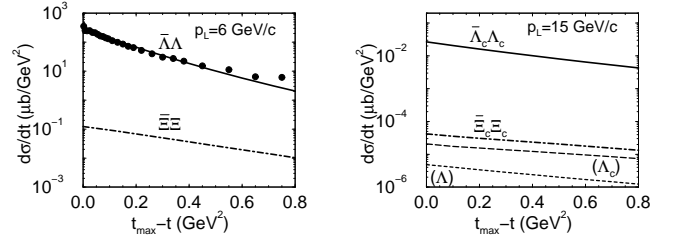


FIG. 4: Left panel: Differential cross section of the reactions $\bar{p}p \rightarrow \bar{\Lambda}\Lambda$ (solid curve) and sum of $\bar{p}p \rightarrow \Xi^-\Xi^-$ and $\bar{p}p \rightarrow \Xi^0\Xi^0$ (dot-dashed curve) as a function of $t_{\text{max}} - t$ for the initial momentum in the laboratory system $p_L = 6$ GeV/c. The experimental data are taken from Ref. [12]. Right panel: Differential cross section of the reactions $\bar{p}p \rightarrow \bar{\Lambda}_c\Lambda_c$ (solid curve) and sum of $\bar{p}p \rightarrow \Xi_c^0\Xi_c^0$ and $\bar{p}p \rightarrow \Xi_c^+\Xi_c^+$ (dot-dashed curve) as a function of $t_{\text{max}} - t$ for the initial momentum $p_L = 15$ GeV/c. The short dashed and dashed curves correspond to separate contributions of intermediate $\bar{\Lambda}\Lambda$ and $\bar{\Lambda}_c^+\Lambda_c^+$ states (cf. Fig. 1 b). For $X_{\text{SU}(4)} = 1$.

by a factor 4-6. In order to understand the reason of such a suppression, in Fig. 5 we present the differential cross sections of all $\bar{Y}Y \rightarrow \bar{Y}'Y'$ processes participating in the formation of $\Xi_c\Xi_c$. Qualitatively, the ratio of

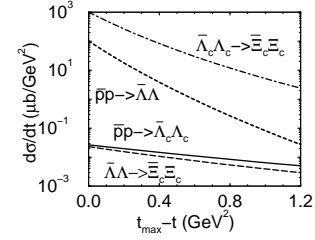


FIG. 5: Differential cross sections of all considered $\bar{Y}Y \rightarrow \bar{Y}'Y'$ processes contributing to the formation of $\Xi_c\Xi_c$ as a function of $t_{\text{max}} - t$ for $p_L = 15$ GeV/c and $X_{\text{SU}(4)} = 1$.

the cross section of $\Xi_c\Xi_c$ production with intermediate $\Lambda_c^+\Lambda_c^+$ and $\Lambda\Lambda$ states at $t \simeq t_{\text{max}}$ would be proportional to $[d\sigma^{\bar{p}p \rightarrow \bar{\Lambda}_c\Lambda_c} \times d\sigma^{\bar{\Lambda}_c\Lambda_c \rightarrow \Xi_c\Xi_c}] / [d\sigma^{\bar{p}p \rightarrow \bar{\Lambda}\Lambda} \times d\sigma^{\bar{\Lambda}\Lambda \rightarrow \Xi_c\Xi_c}]$ multiplied by the kinematical factor $(Q_{\Lambda_c}/Q_{\Lambda})^2 \simeq 0.36$ at $p_L = 15$ GeV. Taking values of corresponding cross sections from Fig. 5 one gets $0.36 \times [2.7 \times 10^{-2} \times 10^3] / [2.3 \times 10^{-2} \times 10^2] \simeq 4.2$, which is in agreement with results exhibited in Fig. 4 (right panel).

In Fig. 6 (left panel) we show the ratio of yields of $\Xi\Xi$ to $\bar{\Lambda}\Lambda$ for charmed and non-charmed hyperons as a function of $t_{\text{max}} - t$ at $p_L = 15$ GeV/c. At $t \sim t_{\text{max}}$ this ratio for charmed hyperons is about an order of magnitude greater. The difference decreases with increasing values of $-t$.

In Fig. 6 (right panel) we show the ratio of the yields of $\Xi_c\Xi_c$ to $\Xi\Xi$ hyperons and of $\bar{\Lambda}_c\Lambda_c$ to $\bar{\Lambda}\Lambda$ hyperons as a function of the SU(4) symmetry violation parameter $X_{\text{SU}(4)}$ for the transferred momentum $t_{\text{max}} - t = 0.2$ GeV². The cross sections of $\bar{p}p \rightarrow \Xi_c\Xi_c$ and $\bar{p}p \rightarrow \bar{\Lambda}_c\Lambda_c$ reactions scale with $X_{\text{SU}(4)}^8$ and $X_{\text{SU}(4)}^4$, re-

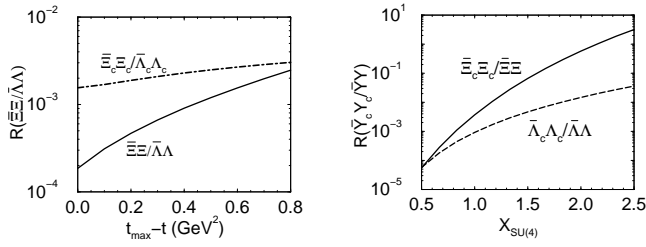


FIG. 6: Left panel: Ratio of yields of $\Xi_c \Xi_c$ to $\bar{\Lambda}_c \Lambda_c$ (dashed curve) and of $\Xi \Xi$ to $\bar{\Lambda} \Lambda$ (solid curve) as a function of $t_{\max} - t$ for $p_L = 15$ GeV/c. Right panel: Ratio of the yields of $\Xi_c \Xi_c$ to $\Xi \Xi$ (solid curve) and of $\bar{\Lambda}_c \Lambda_c$ to $\bar{\Lambda} \Lambda$ (dot-dashed curve) as a function of the SU(4) violation parameter $X_{\text{SU}(4)}$. For $t_{\max} - t = 0.2$ GeV².

spectively. (Here we assume the dominant contribution in $\bar{p}p \rightarrow \Xi_c \Xi_c$ reaction with intermediate $\bar{\Lambda}_c \Lambda_c$ state). Therefore, this ratio for $\Xi \Xi$ hyperons increases much faster with $X_{\text{SU}(4)}$.

Our result for the longitudinal symmetries is shown in Fig. 7. First, let us remind that the longitudinal asymmetry for the one-step reactions (e.g. $\bar{p}p \rightarrow \bar{\Lambda} \Lambda$) is defined by the spin-conserving $A(s)$ and spin-flip $B(s)$ amplitudes as $A = B^2(s)/(A^2(s) + B^2(s))$ [5]. At $t = t_{\max}$ the spin-flip amplitude has a following form

$$B(s) \sim \left(\frac{\mathbf{p}_p}{E + M_p} - \frac{\mathbf{p}_Y}{E + M_Y} \right)^2, \quad (7)$$

where M_Y and \mathbf{p}_Y denote the mass and three-momentum of outgoing hyperon, respectively. In case of $M_Y \sim M_p$ and $\mathbf{p}_Y \sim \mathbf{p}_p$, $B(s) \rightarrow 0$ and the longitudinal asymmetry vanishes (cf. solid curve in Fig. 7 (left panel)). The situation is different for the $\bar{p}p \rightarrow \bar{\Lambda}_c \Lambda_c$ reaction, where $B(s)$ is finite and large, $B^2(s) \gg A^2(s)$: the asymmetry goes to one as it is shown by solid curve in Fig. 7 (right panel). For the loop diagrams the spin-flip part does not vanish even for light hyperons because of the integration over $d\Omega_\Lambda$ and sum over the spin projections in Eq. (1). This leads to a modification of asymmetries as shown by

dot-dashed curves in Fig. 7 for $\Xi \Xi$ and $\Xi_c \Xi_c$ yields. In all considered cases, the longitudinal asymmetries are large enough to be accessible experimentally.

In summary we extend the model [5] for studying the $\Xi \Xi$ and $\Xi_c \Xi_c$ production in peripheral $\bar{p}p$ collisions. The Ξ and Ξ_c hyperons are assumed to be produced in two-step processes, where the first step corresponds to the intermediate $\bar{\Lambda} \Lambda$ ($\bar{\Lambda}_c \Lambda_c$) production, and subsequently the Ξ (Ξ_c) hyperons are formed by the final state interactions $\bar{\Lambda} \Lambda \rightarrow \Xi \Xi$, $\bar{\Lambda} \Lambda \rightarrow \Xi_c \Xi_c$ and $\bar{\Lambda}_c \Lambda_c \rightarrow \Xi_c \Xi_c$ for which we employ the same mechanism as for description of $\bar{p}p \rightarrow \bar{\Lambda} \Lambda$ and $\bar{p}p \rightarrow \bar{\Lambda}_c \Lambda_c$ reactions. We estimated the corresponding differential cross section and longitudinal asymmetries. For a benchmark calculation we assumed the validity of SU(4) symmetry. The $\bar{p}p \rightarrow \Xi_c \Xi_c$ cross section is sensitive to the degree of the SU(4) symmetry violation which is quantified by the ratio of $\Xi_c \Xi_c$ to $\Xi \Xi$ as a function of the SU(4) violation parameter, $X_{\text{SU}(4)}$.

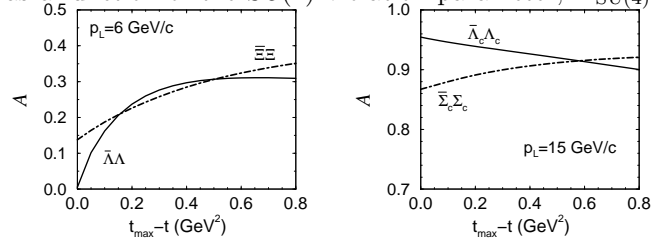


FIG. 7: Longitudinal asymmetry as a function of $t_{\max} - t$. Left panel: $\bar{p}p \rightarrow \bar{\Lambda} \Lambda$ (solid curve) and $\bar{p}p \rightarrow \Xi \Xi$ (dot-dashed curve) at $p_L = 6$ GeV/c. Right panel: $\bar{p}p \rightarrow \bar{\Lambda}_c \Lambda_c$ (solid curve), and $\bar{p}p \rightarrow \Xi_c \Xi_c$ (dot-dashed curve) for $p_L = 15$ GeV/c.

Such a ratio should be determined experimentally in order to fix this important parameter.

Prof. Horst Stöcker is gratefully acknowledged for discussions leading to the present investigation. One of the authors (A.I.T.) appreciates the warm hospitality in Helmholtz-Zentrum Dresden-Rossendorf.

[1] see <http://www.gsi.de/portrait/fair.html>.
[2] M.F.M. Lutz *et al.* (PANDA Collaboration), Physics Performance Report for PANDA: Strong Interaction Studies with Antiprotons, arXiv:0903.3905 [hep-ex].
[3] (Eds.) B. Friman *et al.*, The CBM Physics Book, Lect. Notes Phys. **814**, 1 (2011).
[4] V. Barone *et al.* (PAX Collaboration), arXiv:hep-ex/0505054.
[5] A. I. Titov and B. Kämpfer, Phys. Rev. C **78**, 025201 (2008).
[6] K. G. Boreskov and A. B. Kaidalov, Sov. J. Nucl. Phys. **37**, 100 (1983) [Yad. Fiz. **37**, 174 (1983)].
[7] E. Braaten and P. Artoisenet, Phys. Rev. D **79**, 114005

(2009).
[8] J. Haidenbauer and G. Krein, Phys. Lett. B **687**, 314 (2010).
[9] M. E. Peskin and D. V. Schroeder, *An Introduction to Quantum Field Theory* (Addison-Wesley, Reading, MA, 1996).
[10] M. M. Brisudova, L. Burakovsky and J. T. Goldman, Phys. Rev. D **61**, 054013 (2000).
[11] V. G. J. Stoks and T. A. Rijken, Phys. Rev. C **59**, 3009 (1999).
[12] H. Becker *et al.* (CERN-Munich Collaboration), Nucl. Phys. B **141**, 48 (1978).